



Effect of microsilica content on microstructure and properties of foamed ceramics with needle-like mullite

Wenyong Zhou¹, Wen Yan^{1,2,*}, Nan Li^{1,*}, Yuanbing Li^{1,2}, Yajie Dai^{1,2}, Zheng Zhang¹

¹The State Key Laboratory of Refractories and Metallurgy, Wuhan University of Science and Technology, Wuhan 430081, China

²National-Provincial Joint Engineering Research Center of High Temperature Materials and Lining Technology, Wuhan University of Science and Technology, Wuhan 430081, China

Received 10 November 2018; Received in revised form 18 March 2019; Accepted 13 June 2019

Abstract

In this study, five foamed ceramics with struts containing needle-like mullite were prepared by direct-foaming method using white clay, industrial alumina and microsilica powder as raw materials. The effects of microsilica content on the phase compositions, microstructures and properties of foamed ceramics were investigated. The results showed that the adding of microsilica decreased the average pore size and apparent porosity and increased the compressive strength and thermal conductivity of the foamed ceramics by affecting the properties of foamed slurry and reaction sintering process. The foamed ceramics with 10 wt.% microsilica content showed the best properties with high porosity of 75.8%, positive reheating linear change, compressive strength of 1.44 MPa and low thermal conductivity of 0.219 W/(m·K) (at 350 °C).

Keywords: mullite foamed ceramics, struts containing needle-like mullite, thermal conductivity, refractories

I. Introduction

Foamed ceramics could be used as high-temperature thermal-insulating materials, gas filters and heat exchangers, due to their high porosities, low conductivities and high specific strengths [1–9]. Mullite [10–14] is a well-known refractory material with high resistance to chemical attack, high compressive strength, low thermal conductivity, etc. Thus, mullite foamed ceramics are potential to be used as thermal-insulating linings for high-temperature furnaces. However, foamed ceramics are easily deformed or even damaged during a long-time and high-temperature service, due to the sintering stress and external load [15–17]. In order to solve this problem, there are two methods. One is to prepare the high-densification strut through using micron or nanosized powder as raw materials, which can promote the sintering degree of the strut of foamed ceramics at high temperature and then improve the strengths. For instance, Deng *et al.* [18] prepared the porous mullite ceramics for filter using mullite powder (D_{50} was 2.82 μm), which had a high strength of 15.3 MPa and high porosity of

76%. The other method is based on the preparation of strut containing needle-like mullite [19–21]. For example, Li *et al.* [20] introduced the mullite whiskers into the porous anorthite ceramics and found that the compressive strengths increased by four times. Although both methods can improve the mechanical strength efficiently, the high cost of the nanosized raw material as well as pre-preparation of mullite whisker limited the application of such foamed ceramics in thermal-insulating linings for high-temperature furnaces. On the basis of the analysis above, it is necessary to develop foamed ceramics with high properties as well as low cost.

Compared with the nanosized mullite powder and pre-prepared mullite whiskers, white clay, industrial alumina and microsilica, which are very often used as raw materials for refractories, are cheaper. In addition, the clay and microsilica can enhance the strength of the strut of foamed ceramics, because their nanosized particles promote the sintering densification through increasing the packing density of powder in green specimen. Furthermore, the impurities of clay, such as K_2O and Na_2O , would facilitate the formation of needle-like mullite through dissolution-precipitation mechanism, which

*Corresponding author: tel: +86 27 68862511, e-mail: yanwen@wust.edu.cn

is beneficial to improve the strength and thermal shock resistance of the foamed ceramics [22,23].

In addition to the density and crystal morphology of strut, reserving a small amount of free Al_2O_3 and SiO_2 in the strut is probably another way to improve the strength of foamed ceramics [24], as free Al_2O_3 and SiO_2 could transform into mullite showing a volume expansion to counteract the sintering shrinkage [25–31]. In our previous work [24], 18.0 wt.% corundum and 4.7 wt.% quartz were remained in the mullite foamed ceramics, which have a 0.11% reheating linear change after reheating at 1500 °C. In present work, the particle size of alumina was bigger than that of the white clay and microsilica, which slowed down the sintering velocity and reserved a bit of corundum. Under these conditions the corundum would react with microsilica to form mullite with a lot expansion during the service life, and counteract the sintering shrinkage.

The aim of the present work was to prepare foamed ceramics with majority of needle-like mullite, corundum and minor cristobalite, using white clay, industrial alumina and microsilica as raw materials. The corundum and minor cristobalite reserved in the foamed ceramics were used to form mullite in situ to sustain the thermo-mechanical stress caused by sintering and external load during service. The effect of the microsilica content on the microstructure and properties of the foamed ceramics was investigated in detail.

II. Experimental procedure

2.1. Experimental materials

Industrial alumina (average particle size was 52.28 μm , Guangming Gaoke Co., China), white clay (average particle size was 1.73 μm , Guangming Gaoke Co., China) and microsilica (average particle size was 1.25 μm , Elkem Co., Norway) were used as raw materials and their chemical compositions were listed in Table 1. Sodium dodecyl sulfate (SDS, chemical purity, Sinapharm Chemical Reagent Co. Ltd., China) was used as foaming agent. Carboxymethyl cellulose sodium (CMC, chemical purity, Sinapharm Chemical Reagent Co. Ltd., China) and sodium tripolyphosphate (STP, Sinapharm Chemical Reagent Company, China) were selected as foam stabilizing agent and dispersing agent, respectively.

Table 1. Chemical composition of the raw materials in wt. %

	SiO_2	Al_2O_3	Fe_2O_3	CaO	MgO	K_2O	Na_2O	TiO_2	IL
White clay	49.71	31.92	1.45	0.14	0.15	0.17	0.21	2.10	13.73
Industrial alumina	-	98.26	-	-	-	-	0.32	-	1.36
Microsilica	97.09	0.06	0.11	0.15	0.16	0.38	0.05	0.02	1.70

Table 2. Compositions of five powder mixtures in wt. %

	S0	S5	S10	S15	S20
Industrial alumina	58.0	55.1	52.2	49.3	46.4
White clay	42.0	39.9	37.8	35.7	33.6
Microsilica	0.0	5.0	10.0	15.0	20.0

2.2. Specimen preparation

Five initial powder mixtures with different microsilica content were obtained by mixing industrial alumina, white clay and microsilica (Table 2). Subsequently, the slurries containing 55 wt.% powder mixture, 0.30 wt.% SDS, 0.15 wt.% CMC, 0.25 wt.% STP and 44.30 wt.% deionized water were initially prepared via mechanical mixing by a household hand mixer at lower speed of 800 r/min for 1 min. The initial slurries were then stirred for 5 min using a household hand mixer at the speed of 1300 r/min to obtain foamed slurries. The foamed slurries were cast in rectangle parallelepiped specimens (150 mm \times 40 mm \times 40 mm) and disc specimens (\varnothing 180 mm \times H20 mm). After being cured for 24 h at room temperature, all specimens were dried at 110 °C for 24 h. Then the dried disc and parallelepiped specimens were fired at 1500 °C for 3 h in an electric furnace before they cooled down to room temperature.

2.3. Characterization methods

The chemical compositions of the raw materials were determined by an inductively coupled plasma-atomic emission spectrometry according to the Chinese standard GB/T 6900-2006. The median particle size was measured by a laser size analyser (Mastersizer 2000, Malvern Instruments Ltd, UK).

The density of foamed slurry (*FSD*) and the volume expansion of foamed slurry (*FSVE*) were calculated by the following equations: $FSD = m/v_1$, $FSVE = v_1/v_0$, wherein m denoted the mass of the foamed slurry, v_1 denoted the volume of the foamed slurry, v_0 denoted the volume of the initial slurry.

The phase composition was analysed using an X-ray diffractometer (XRD, X'pert Pro, Philips) with $\text{Cu K}\alpha$ radiation ($\lambda = 1.54187 \text{ \AA}$). The XRD pattern was recorded in the 2θ range of 10–90° with a scanning speed of 2°/min, and JCPDS cards no. 01-083-1881, No. 00-042-1468 and No.01-071-0785 were used for the identification of mullite, corundum and cristobalite, respectively. The crystal phase relative contents were calculated using the SemiQuant Mode of the Highscore Plus software (version 3.0) based on the XRD results. The content and the viscosity of the theoretical liquid phase at 1500 °C were calculated by the software FactSage (version 6.2), based on the system of $\text{MgO-Al}_2\text{O}_3\text{-SiO}_2\text{-CaO-Fe}_2\text{O}_3\text{-TiO}_2\text{-K}_2\text{O-Na}_2\text{O}$.

The microstructures and compositions were observed by a scanning electron microscopy (SEM, ISM-6610, JEOL, Japan) with an energy dispersive spectrometer (EDS, QUANTAX200-30, BRUKER Company, Germany). The pore size distributions were statistically analysed through an image analysis method.

The bulk densities and apparent porosities of the fired specimens were measured based on Archimedes' method using water as medium. The compressive strengths were measured by a universal testing machine (ETM, Wance, China) with a loading rate of 0.05 MPa/s.

The reheating linear change (*RLC*) was measured according to the Chinese standard GB/T 5988-2007. For that purpose, the fired specimens were reheated at 1500 °C for 3 h in an electric chamber furnace, which then cooled naturally to room temperature. The *RLC* was calculated by the following equation: $RLC = (L_2 - L_1)/L_1 \times 100\%$, wherein L_1 denoted the length of the fired specimen before reheating, L_2 denoted the length of the fired specimen after reheating.

Thermal conductivities of the fired disc specimens were determined using a water-cooled calorimeter (PBD-30, Sinosteel Luoyang Institute of Refractories Research Co. Ltd., China) according to the Chinese standard YB/T 4130-2005.

III. Results

3.1. Properties of the foam slurries

The effect of microsilica content on the volume expansion (*FSVE*) and the density of the foamed slurries (*FSD*) was shown in Fig. 1. With the increasing of microsilica content from 0 to 20 wt.%, the *FSVE*

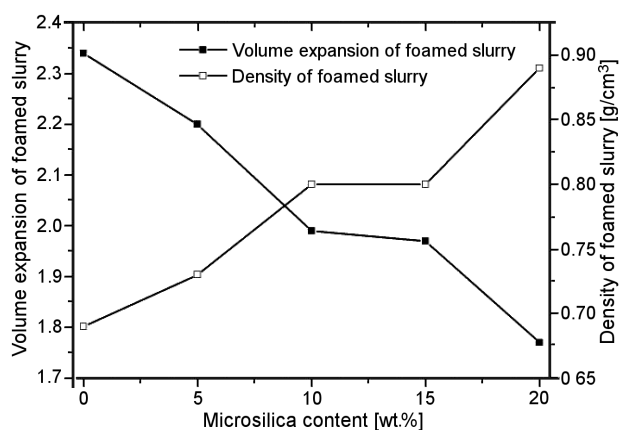


Figure 1. Densities and volume expansions of the foamed slurries with different microsilica content

Table 3. Crystal phase relative compositions of the fired specimens in wt.%

Microsilica content	Mullite	Corundum	Cristobalite
0	72.5	26.7	0.9
5	73.1	25.9	1.0
10	80.3	18.3	1.4
15	78.5	17.2	4.3
20	74.1	19.0	6.9

decreased from 2.34 to 1.77, while the *FSD* increased from 0.69 to 0.89 g/cm³.

3.2. Structure of the fired specimens

XRD patterns of the fired specimens were shown in Fig. 2. The five specimens all consisted mainly of mullite, corundum and minor cristobalite. According to the XRD results, the crystal phase relative content of each specimen was calculated, as listed in Table 3. It was found that with the increasing in the microsilica content, the mullite relative content in the fired specimens increased first, then decreased. When the microsilica content was 10 wt.%, the mullite relative content reached maximum. Meanwhile, with the microsilica content increasing, the relative content of corundum decreased and the relative content of cristobalite increased.

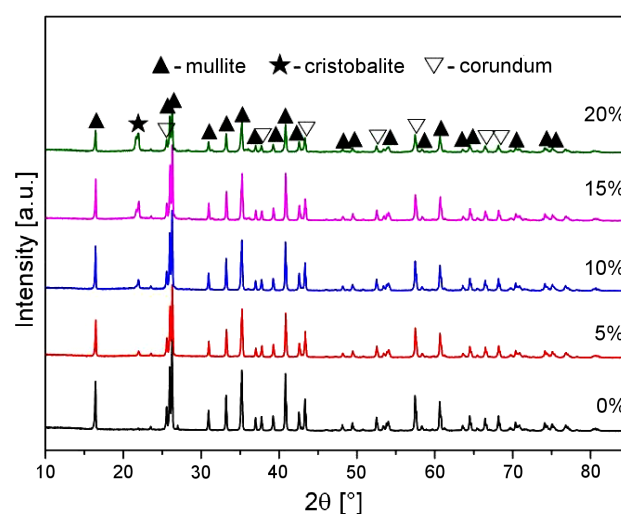


Figure 2. XRD patterns of the fired specimens with different microsilica content

The microstructures of the polished and fractured sections of the fired specimens with different microsilica content were shown in Fig. 3. It can be seen from the polished sections that there were two kinds of pores in the microstructures. One was intra-strut pores, caused from the packing behaviour and the agglomerate of raw materials during sintering process. The other was the inter-strut pores, coming from the foams. With an increase of microsilica content to 20 wt.%, the area fraction of the inter-strut pores decreased, and the inter-strut pores became more uniform and their sizes decreased obviously.

From the microstructures of the fractured sections, it can be seen that the struts of all specimens consisted mostly of mullite. When the microsilica content was less

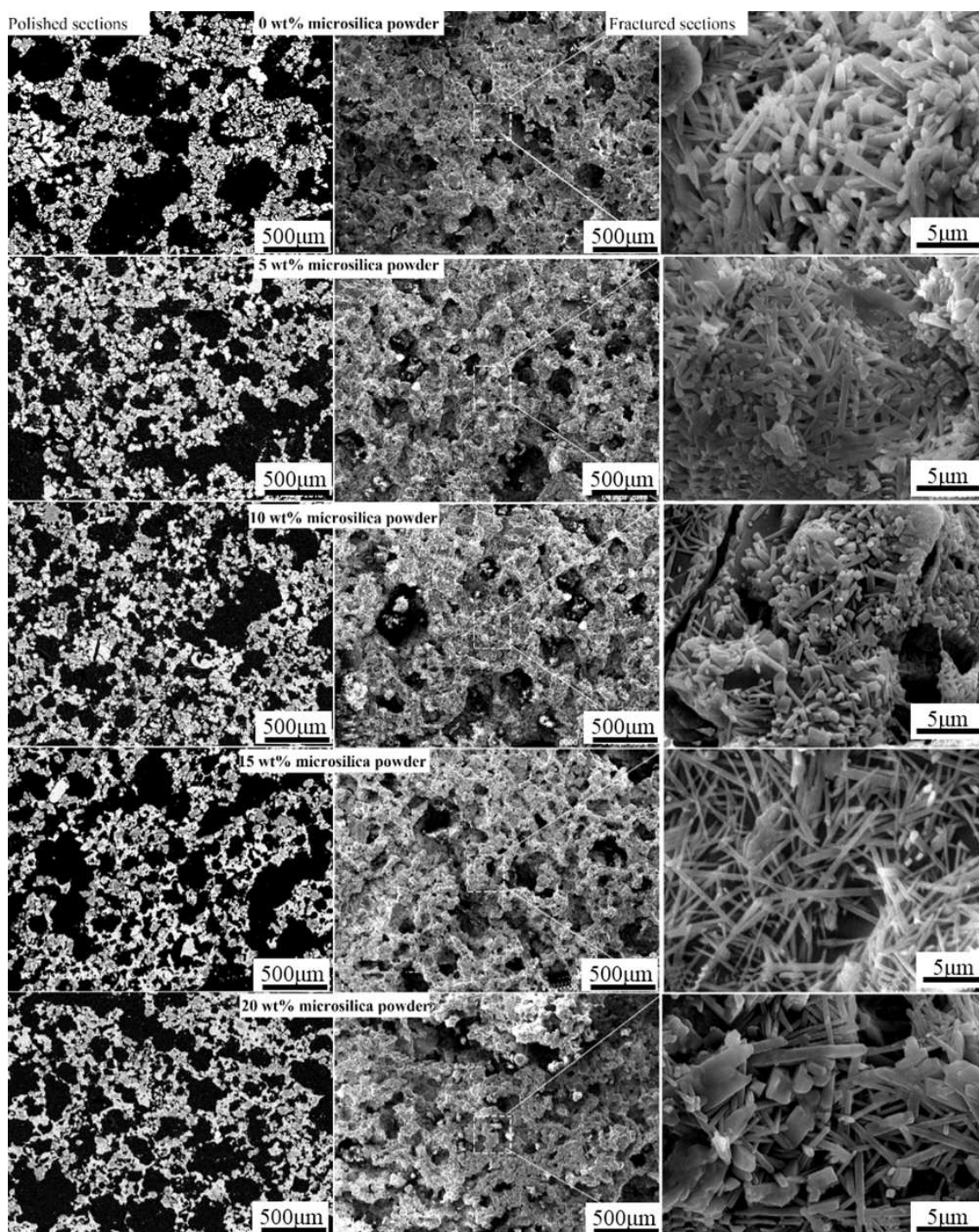


Figure 3. SEM images of specimens with various microsilica content

than 5 wt.%, the main morphology of the mullite was needle-like. By further increasing the microsilica content to 10 wt.% and 15 wt.%, a large number of mullite whiskers with bigger length-diameter ratio in the struts was formed, and some mullite whiskers grew through the micro-pore to form interlock structure. When the microsilica addition was 20 wt.%, a large number of pillared mullite grains was formed, whose average length-diameter ratio was only 7.73.

In order to investigate the inter-strut and intra-strut pore characteristics, the pore size distributions of the

fired specimens were shown in Fig. 4. The bimodal pore size distributions were observed in all specimens, with intra-strut and inter-strut pore peaks in the ranges of 0–200 μm and 600–1000 μm, respectively. With an increase of the microsilica content from 0 to 20 wt.%, for the inter-strut pores, the peak values decreased and the curves shifted towards the left, which suggested that the inter-strut pore area fraction decreased. For the intra-strut pores, the intensity of the peak values increased. In addition, the curves of cumulative porous area versus pore size were shown in Fig. 5. With increasing mi-

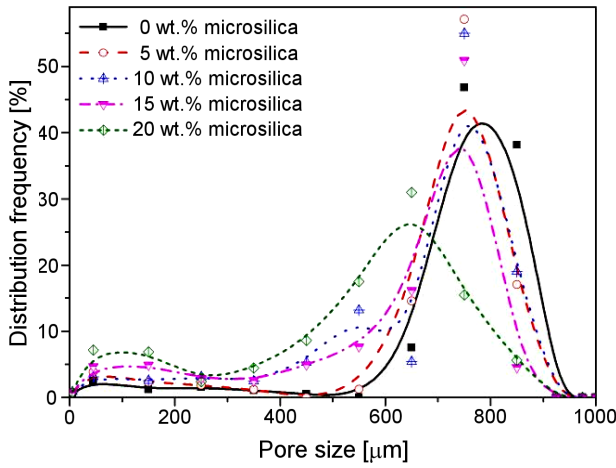


Figure 4. Pore size distribution of the fired specimens with various microsilica content

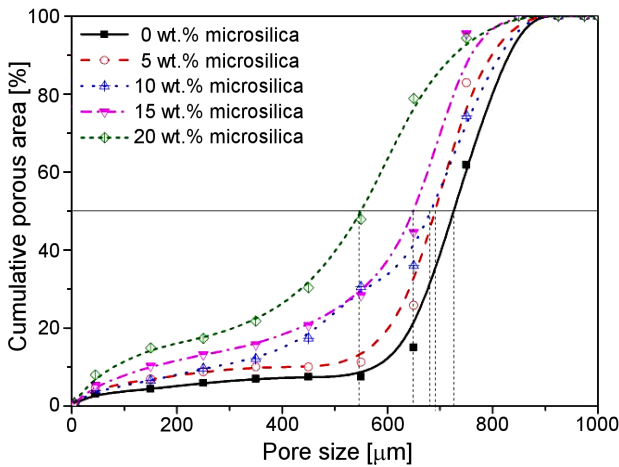


Figure 5. Cumulative porous area as a function of pore size of the fired specimen with different microsilica content

microsilica content from 0 to 20 wt.%, the curves shifted markedly towards the left and the medium pore size declined from 726 μm to 550 μm. These results proved that though the increasing of the microsilica content decreased the inter-strut pore area fraction and the porosity, it can indeed reduce the pore size of foamed ceramics.

3.3. Properties of the fired specimens

The physical properties of the fired specimens were listed in Table 4. With an increase of microsilica content from 0 to 20 wt.%, although the apparent porosities decreased from 78.4% to 69.4%, the compressive

strengths of the fired specimens increased obviously from 0.59 to 4.31 MPa.

The microsilica content also strongly affected the reheating linear changes. As listed in Table 4, with an increase of the microsilica content from 0 to 10 wt.%, the reheating linear changes of the fired specimens decreased from 0.15% to 0.12%, which indicated that the volume of the fired specimens would expand slightly in the future service. By further increasing the microsilica content to 20 wt.%, the reheating linear change decreased to -0.51%, and it possibly could lead to the shrinkage deformation of the foamed ceramics in the future service.

The thermal conductivities of the fired specimens at various testing temperatures were shown in Fig. 6. When the testing temperatures were the same, the thermal conductivities increased with an increase of the microsilica content. For example, at 200 °C, the thermal conductivities increased from 0.163 W/(m·K) to 0.259 W/(m·K) with increasing the microsilica content from 0 to 20 wt.%. For any of the five specimens, the thermal conductivities increased as the testing temperature increased. When the testing temperature was 800 °C, the maximum thermal conductivity of the specimen with 20 wt.% microsilica content was 0.384 W/(m·K).

IV. Discussion

Based on the above results, it can be concluded that the foamed ceramics with struts containing needle-like

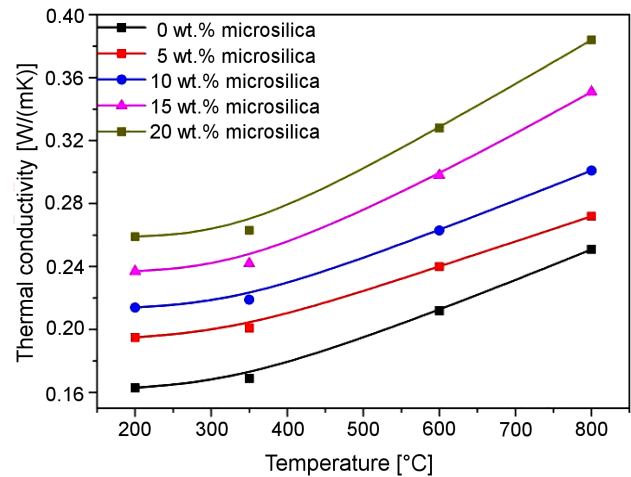


Figure 6. Thermal conductivities of the specimens with different microsilica contents vs. testing temperature

Table 4. Properties of the fired samples with various microsilica content

Microsilica content [wt.%]	Apparent porosity [%]	Bulk density [g/cm ³]	Compressive strength [MPa]	Reheating linear [%]
0	78.4	0.67	0.59	0.15
5	77.5	0.68	0.62	0.14
10	75.8	0.71	1.44	0.12
15	73.7	0.75	2.4	-0.23
20	69.4	0.86	4.31	-0.51

mullite were successfully fabricated, and the optimized product was a specimen with 10 wt.% microsilica content. The effect of microsilica content on the microstructures and properties of the specimens should be considered from two stages: the preparation stage of the foamed slurry and the sintering stage of the specimens.

In the preparation of the foamed slurry, the microsilica had smaller particle size and higher specific surface area than white clay and industrial alumina, which increased the viscosities of slurries [32]. The higher viscosity could prevent the air from entering the slurry, and thus *FSVE* decreased and the *FSD* increased (Fig. 1). Additionally, the higher slurry viscosity increased the stability of the foamed slurry, and thus reduced the average pore sizes of the green specimens, which set in place a microstructure trajectory that controlled the final pore characteristics of the fired specimens.

In the sintering stage of the specimens, the microsilica powder affected the microstructure of the strut in two ways: one was to react with industrial alumina to form more mullite; the other was to form liquid phase and then promote liquid reaction sintering.

For the formation of the mullite, there are two ways. The one was decomposition of white clay to form the primary mullite [33], which was the same no matter whether microsilica is added or not. Another was the precipitation of the secondary mullite with needle-like morphology from the local silica-rich liquid phase. In this process, according to dissolving-precipitation mechanism [34], the formation of the secondary mullite was controlled by the dissolution velocity of Al_2O_3 into the silica-rich liquid phase [35]. With the increasing of microsilica content to 10 wt.%, the silica-rich liquid content increased (Fig. 7), and then accelerated dissolution of Al_2O_3 , which was beneficial for the formation of needle-like mullite. However, when the microsilica content reached 20 wt.%, the excessive SiO_2 dissolved into silica-rich liquid. This improves the viscosity of liquid phase (Fig. 7) and slows down diffusion velocity of Al^{3+} and SiO_4^{4-} ions, which prevented the precipitation of the secondary mullite (Fig. 3).

For the formation of the liquid, impurities of the clay such as Fe_2O_3 and TiO_2 would react with alumina to form the liquid phase (Fig. 7). However, the content of impurities varied slightly with increasing microsilica content, so the variable SiO_2 content was a more important factor affecting the liquid phase content. Thus, an increase of microsilica content from 0 to 20 wt.% increases the liquid phase content (Fig. 7), and then promotes liquid reaction sintering and improves the densification of the struts. The compressive strengths of the

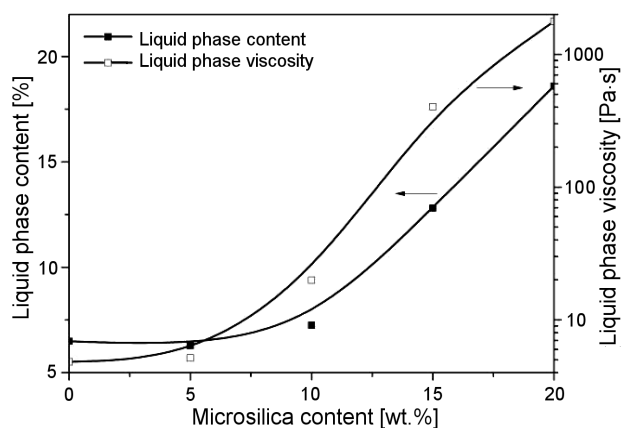


Figure 7. Content and viscosity of the liquid phase of the samples with different microsilica contents fired at 1500 °C

specimens improved due to the denser struts and the formation of the needle-like mullite. Additionally, the liquid phase also strongly affected the reheating linear changes. When the microsilica content was lower than 10 wt.%, there was a small amount of the liquid phase, which would react with corundum to form mullite with volume expansion during the reheating process and counteract the sintering shrinkage. However, further increasing of microsilica content to 15 wt.% and 20 wt.%, the excessive liquid phase was formed, as shown in Fig. 7. When the shrinkage caused by liquid reaction sintering exceeded the expansion caused by the formation of mullite *in situ*, the shrinkage occurred during reheating. Therefore, when the microsilica content was higher than 15 wt.%, the reheating linear change was negative, which was adverse during the high-temperature service.

Thermal conductivity was dependant on the phase compositions and pore characteristics of the specimens. In this study, the increase of thermal conductivities was obtained with increasing of microsilica content. However, with the increase of microsilica content the content of cristobalite with lower conduction coefficient increased and the content of corundum with higher conduction coefficient decreased. Thus, it can be concluded that the lower porosity contributes more to the increase of thermal conductivities of the foamed ceramics.

Additionally, Table 5 compared the porous mullite-based ceramics prepared from different raw materials. It is apparent that compared with the mullite foamed ceramics prepared by mullite fibres, the mullite foamed ceramics in this study has a higher compressive strength and a lower thermal conductivity, which is beneficial to prolong the service life. Similarly, apart from the higher compressive strength, the specimen had higher poros-

Table 5. Properties of the fired samples with various microsilica content

Raw materials	Sintering condition	Porosity [%]	Compressive strength [MPa]	Thermal conductivity [W/(m·K)]	Reference
Mullite fibres	1600 °C/4 h	79.3	1.22	0.449	[36]
$\text{SiO}_{1.51}\text{C}_{4.03}\text{H}_{4.06}, \text{Al}_2\text{O}_3$	1600 °C/4 h	73	1.1	-	[37]
Alumina, clay, microsilica	1500 °C/3 h	75.8	1.44	0.214	Present work

ity than the ceramics fabricated by $\text{SiO}_{1.51}\text{C}_{4.03}\text{H}_{4.06}$ and Al_2O_3 . In addition, it is worth mentioning that, the shorter sintering time and the lower sintering temperature in the present work were conducive to resources saving and environmental protection.

V. Conclusions

The low-cost foamed ceramics with struts containing needle-like mullite for the lining of high-temperature furnace were developed successfully in this paper. The effect of microsilica content on the phase compositions, microstructure, compressive strength and thermal conductivity was investigated. The following conclusions can be reached:

1. The adding of the microsilica decreased the volume expansion of foamed slurry and average pore sizes of the green specimens, which set in place a microstructure trajectory that controlled the final pore characteristics of the fired samples.
2. Due to the microsilica addition, the sinterability and densification of the struts increased, the porosity decreased and the thermal conductivity increased, while the compressive strength was obviously improved.
3. The optimized product was a specimen with 10 wt.% microsilica content which had high porosity of 75.8%, positive reheating linear change, compressive strength of 1.44 MPa and thermal conductivity of 0.219 W/(m·K) (at 350 °C).

Acknowledgement: This work was financially supported by the National Key R&D Program of China (Grant No. 2017YFB0310701).

References

1. W. Yan, G. Wu, S. Ma, S. Schafföner, Y. Dai, Z. Chen, J. Qi, N. Li, “Energy efficient lightweight periclase-magnesium alumina spinel castables containing porous aggregates for the working lining of steel ladles”, *J. Eur. Ceram. Soc.*, **38** (2018) 4276–4282.
2. J. Liu, Y. Li, Y. Li, S. Sang, S. Li, “Effects of pore structure on thermal conductivity and strength of alumina porous ceramics using carbon black as pore-forming agent”, *Ceram. Int.*, **42** (2016) 8221–8228.
3. N. Xu, S. Li, Y. Li, Z. Xue, L. Yuan, J. Zhang, L. Wang, “Preparation and properties of porous ceramic aggregates using electrical insulators waste”, *Ceram. Int.*, **41** (2015) 5807–5811.
4. K. Huang, Y. Li, S. Li, R. Xiang, “Preparation and properties of alumina foams via thermally induced foaming of molten D-glucose monohydrate”, *J. Porous Mater.*, **24** (2017) 121–128.
5. K. Huang, Y. Li, Y. Zhao, S. Li, Y. Li, S. Sang, “Effects of foaming temperature on the preparation and microstructure of alumina foams”, *Mater. Lett.*, **165** (2016) 19–21.
6. K. Huang, Y. Li, S. Li, L. Wang, S. Wang, “Effects of microsilica addition on the microstructure and properties of alumina foams”, *Ceram. Int.*, **42** (2016) 16401–16404.
7. L. Zhu, S. Li, Y. Li, N. Xu, “Novel applications of waste ceramics on the fabrication of foamed materials for exterior building walls insulation”, *Const. Build. Mater.*, **180** (2018) 291–297.
8. W. Yan, J. Chen, N. Li, B. Han, Y. Wei, “Lightweight cordierite-mullite refractories with low coefficients of thermal conductivity and high mechanical properties”, *Bull. Mater. Sci.*, **38** [2] (2015) 409–415.
9. Z. Wu, L. Sun, J. Pan, J. Wang, “Highly porous Y_2SiO_5 ceramic with extremely low thermal conductivity prepared by foam-gelcasting-freeze drying method”, *J. Am. Ceram. Soc.*, **101** [3] (2018) 1042–1047.
10. W. Yan, N. Li, B.Q. Han, “Effects of sintering temperature on pore characterization and strength of porous corundum-mullite ceramics”, *J. Ceram. Process. Res.*, **11** [3] (2010) 388–391.
11. W. Yan, H. Luo, J. Tong, N. Li, “Effects of sintering temperature on pore characterization and strength of porous cordierite-mullite ceramics by a pore-forming in-situ technique”, *Int. J. Mater. Res.*, **103** [10] (2012) 1239–1243.
12. W. Yan, N. Li, “Pore-size distribution and strength of porous mullite ceramics”, *Am. Ceram. Soc. Bull.*, **85** [12] (2006) 9401–9406.
13. W. Yan, N. Li, B. Han, “A study of the development of crystal shape of mullite prepared from $\text{Al}(\text{OH})_3$ and kaolinite gangue”, *J. Ceram. Process. Res.*, **11** [6] (2010) 733–735.
14. W. Yan, Q. Chen, X. Lin, N. Li, “Pore characteristics and phase compositions of porous corundum-mullite ceramics prepared from kaolinite gangue and $\text{Al}(\text{OH})_3$ with different amount of CaCO_3 addition”, *J. Ceram. Soc. Jpn.*, **123** (2015) 897–902.
15. A. Malfliet, S. Lotfian, L. Scheunis, V. Petkov, L. Pande-laers, P.T. Jones, B. Blanpain, “Degradation mechanisms and use of refractory linings in copper production processes: A critical review”, *J. Eur. Ceram. Soc.*, **34** (2014) 849–876.
16. F. Damhof, W. Brekelmans, M. Geers, “Predictive FEM simulation of thermal shock damage in the refractory lining of steelmaking installations”, *J. Mater. Process. Technol.*, **211** (2011) 2091–2105.
17. C. Yeh, C. Ho, R. Yang, “Conjugate heat transfer analysis of copper staves and sensor bars in a blast furnace for various refractory lining thickness”, *Int. Comm. Heat Mass Tran.*, **39** (1933) 58–65.
18. X. Deng, J. Wang, J. Liu, H. Zhang, F. Li, H. Duan, L. Lu, Z. Huang, W. Zhao, S. Zhang, “Preparation and characterization of porous mullite ceramics via foam-gelcasting”, *Ceram. Int.*, **41** (2015) 9009–9017.
19. F. Han, Z. Zhong, Y. Yang, W. Wei, F. Zhang, W. Xing, Y. Fan, “High gas permeability of SiC porous ceramics reinforced by mullite fibers”, *J. Eur. Ceram. Soc.*, **36** (2016) 3909–3917.
20. C. Li, C. Bian, Y. Han, C.A. Wang, L. An, “Mullite whisker reinforced porous anorthite ceramics with low thermal conductivity and high strength”, *J. Eur. Ceram. Soc.*, **36** [3] (2016) 761–765.
21. S. Li, H. Du, A. Guo, H. Xu, D. Yang, “Preparation of self-reinforcement of porous mullite ceramics through in situ synthesis of mullite whisker in flyash body”, *Ceram. Int.*, **38** [2] (2012) 1027–1032.
22. M. Wu, G.L. Messing, “Fabrication of oriented SiC-whisker-reinforced mullite matrix composites by tape casting”, *J. Am. Ceram. Soc.*, **77** (1994) 2586–2592.

23. Z. Zhu, Z. Wei, J. Shen, L. Zhu, L. Xu, Y. Zhang, S. Wang, T. Liu “Fabrication and catalytic growth mechanism of mullite ceramic whiskers using molybdenum oxide as catalyst”, *Ceram. Int.*, **43** (2017) 2871–2875.
24. W. Zhou, W. Yan, N. Li, Y. Li, Y. Dai, B. Han, Y. Wei, “Preparation and characterization of mullite foam ceramics with porous struts from white clay and industrial alumina”, *Ceram. Int.*, **44** (2018) 22950–22956.
25. R.J. Galán-Arboledas, M. Cotes-Palomino, S. Bueno, C. Martínez-García, “Evaluation of spent diatomite incorporation in clay based materials for lightweight bricks processing”, *Const. Build. Mater.*, **144** (2017) 327–337.
26. V. Silva, M. Silva, W. Gonçalves, R.R. Menezes, G. Araújo Neves, H. Lucena Lira, L.N. Lima Santana, “Porous mullite blocks with compositions containing kaolin and alumina waste”, *Ceram. Int.*, **42** (2016) 15471–15478.
27. B. Lin, J. Liu, N. Zhou, “Sillimanite, kyanite and andalusite in China and their applications Part II: Their applications in refractories to improve resistance to creep and thermal shock”, *Chinas Refractories*, **14** [2] (2005) 16–22.
28. H. Guo, W. Li, “Effects of Al₂O₃, crystal types on morphologies, formation mechanisms of mullite and properties of porous mullite ceramics based on kyanite”, *J. Eur. Ceram. Soc.*, **37** (2017) 679–686.
29. M. Sacks, J. Pask, “Sintering of mullite-containing materials: I, Effect of composition”, *J. Am. Ceram. Soc.*, **65** [2] (1982) 65–70.
30. T. Sato, M. Shizuka, M. Shimada, “Sintering and characterization of mullite alumina composites”, *Ceram. Int.*, **12** (1986) 61–65.
31. K. Mazdiyasi, L. Brown, “Synthesis and mechanical properties of stoichiometric aluminum silicate (mullite)”, *J. Am. Ceram. Soc.*, **55** (2010) 548–552.
32. H. Ghaedi, M. Ayoub, S. Sufian, A.M. Shariff, B. Lal, “The study on temperature dependence of viscosity and surface tension of several phosphonium-based deep eutectic solvents”, *J. Mol. Liq.*, **241** (2017) 500–510.
33. A. Raju, V. Lakshmi, R. Prataap, V.G. Resmi, T.P.D. Rajan, C. Pavithran, V.S. Prasad, S. Mohan, “Adduct modified nano-clay mineral dispersed polystyrene nanocomposites as advanced corrosion resistance coatings for aluminum alloys”, *Appl. Clay Sci.*, **126** (2016) 81–88.
34. Q. Fan, H. Chai, Z. Jin, “Dissolution-precipitation-substitution mechanism of self-propagating high-temperature synthesis of β -NiAl(Cu)/ α (Cu,Ni) composite”, *Intermetallics*, **10** [6] (2002) 541–554.
35. Y.F. Chen, M.C. Wang, M.H. Hon, “Phase transformation and growth of mullite in kaolin ceramics”, *J. Eur. Ceram. Soc.*, **24** [8] (2004) 2389–2397.
36. X. Hou, Z. Liu, Z. Liu, L. Yuan, J. Yu, “Porous fibrous ZrO₂-mullite ceramics prepared via tert-butyl alcohol-based gel-casting”, *Ceram. Int.*, **44** (2018) 13580–13587.
37. T. Konegger, R. Felzmann, B. Achleitner, D. Brouczek, “Mullite-based cellular ceramics obtained by a combination of direct foaming and reaction bonding”, *Ceram. Int.*, **41** (2015) 8630–8636.